NJC

Accepted Manuscript

This is an *Accepted Manuscript*, which has been through the Royal Society of Chemistry peer review process and has been accepted for publication.

Accepted Manuscripts are published online shortly after acceptance, before technical editing, formatting and proof reading. Using this free service, authors can make their results available to the community, in citable form, before we publish the edited article. We will replace this *Accepted Manuscript* with the edited and formatted *Advance Article* as soon as it is available.

You can find more information about *Accepted Manuscripts* in the Information for Authors.

Please note that technical editing may introduce minor changes to the text and/or graphics, which may alter content. The journal's standard Terms & Conditions and the Ethical guidelines still apply. In no event shall the Royal Society of Chemistry be held responsible for any errors or omissions in this *Accepted Manuscript* or any consequences arising from the use of any information it contains.

ROYAL SOCIETY OF CHEMISTRY

www.rsc.org/njc

Structure, Photoluminescence and Influence of Temperature in Energy Transfer in Green-emission Phosphor $Ca_9La(GeO_4)_{0.75}(PO_4)_6$: Ce^{3+},Tb^{3+}

Wenjin Xu, Xin Ding, Yuhua Wang*

Key Laboratory for Special Function Materials and Structure Design of the Ministry of the Education, School of Physical Science and Technology, Lanzhou University, Lanzhou, 730000, PR China

*Corresponding author's email: wyh@lzu.edu.cn

Tel.: +86 931 8912772; fax: +86 931 8913554.

Abstract

In order to explore a new phosphors, $Ca_9La(GeO_4)_{0.75}(PO4)_6$ was investigated to get deeper understand to its synthesis and crystal structure. Ce^{3+}/Tb^{3+} co-doped $Ca_9La(GeO_4)_{0.75}(PO_4)_6$ green phosphor was successfully synthesized with the objective of application in ultraviolet-based light-emitting diodes. The characteristic photoluminescence properties were analysed by photoluminescence excitation (PLE) spectra, emission (PL) spectra and decay times. $Ca_9La(GeO_4)_{0.75}(PO_4)_6$ offers high thermal stability in green-emission area. Instead of thermal quenching, with the increasing of the temperature, the intensity of Tb^{3+} shows slightly increase. In order to reasonably explain this special phenomenon, an implicit mechanism between thermal quenching and energy transfer is proposed based on the configurational coordinate diagram. This mechanism could be helpful for the understanding of the thermal properties of multiple activators Ce^{3+} and Tb^{3+} co-doped phosphors as reference.

Introduction

As an ideal environmental friendly candidate, white light-emitting diode (w-LED) has attached much attention [1-3], for its high efficient, compact and has a long lifetime, and has gradually replaced most conventional light sources for these advantages [3,4.5]. To achieve w-LED, the union of UV LED chips and RGB (red, green, blue) phosphor [6] has been widely accepted. However, this method remains many problems of RGB phosphor, among which the most important is that emission intensity of green phosphor reduces rapidly at high temperature [6,8]. This weakness should be improved to enhance the stability of green phosphor.

The intensity of green emission is significantly influenced by its excitation source. To enhance emission intensity, there are several steps to be followed. Firstly, UV-LED chip and phosphor should be matched. Secondly, the emission of chip should be able to be used effectively. According to other reports, there are fewer phosphors suited AlGaN chips. The AlGaN chip presents two peaks at 280nm and 310nm with a rejection of visible light of four decades [9].

In order to acquire the stable green emission, researchers pay attention to Tb^{3+}, since its excition and absorption are stable. Unfortunately, because of its fixed levels, the absorption line of Tb^{3+} in UV area consist of several peaks, which makes the matching of emission of chip even harder. [10,11] One of the solution of using Tb^{3+} emission more effectively is to utilize the energy transfer from sensitizer (Eu^{3+}, Ce^{3+} etc.) to Tb^{3+} [10-14]. Among all the sensitizer, Ce^{3+} acts as a highly efficient emission centre since its 4f-5d transition is allowed by the Laporte parity selection rule[12]. This property has been widely used in many host to improve the emission intensity of Tb^{3+}, such as YPO_4 [11], $LaPO_4$[12], $Ca_6Ba(PO_4)_4O$[13], $Ca_2Al_3O_6F$[14] and $Ca_2Al_2SiO_7$[15]. The combination of Ce^{3+} and Tb^{3+} in one host will perfectly meet the emission of AlGaN chip. However, different Ce^{3+}, Tb^{3+} co-doped luminescent materials show totally different emission intensity, as structure of hosts significantly impact expression of luminescence centre. Most of them are familiar for its low thermo-stability, such as $CaAl_2O_4$[16], $Ca_3Y(GaO)_3(BO_3)_4$[17] and $Ca_4Y_6(SiO_4)_6O$[18]. In order to obtain a thermo-stable green emission, it is necessary to find a new host which is able to avoid losing emission in high temperature. Meanwhile, this improvement should be able to be explained by the mechanism.

Recently, oxide phosphors attract widespread attention because of its high efficiency, low cost and environment friendly property [17-21].

As an important family of oxides, apatite contains a large number of inorganic substance with the formula $M_3(AO_4)_2$. Where M is a univalent to trivalent cation including Na^+, K^+, Ca^{2+}, Sr^{2+}, Ba^{2+}, Cd^{2+}, La^{3+} and so on, A is always P^{5+}, V^{5+}, Si^{4+}, Ge^{4+} and other ion [18]. In all kinds of apatite, β-$Ca_3(PO4)_2$ has been paid much attention [22]. The large quantity of substituted possibilities of β-$Ca_3(PO_4)_2$ creates many kinds of β-$Ca_3(PO_4)_2$-type structure. For instance, $Ca_9Ln(PO_4)_7$-type (CLP) structure, as one of the most attractive β-$Ca_3(PO_4)_2$-type crystal, shows many possibilities, since the Ln^{3+} can be changed to each lanthanide elements[21,22]. Different Ln^{3+} with same doped ion brings different emission [23]. Since La^{3+} has the largest radius (1.06 Å) among all lanthanide elements, it will offer more space for doped RE ions. Besides this, when the larger ion (Ge 1.22 Å) dopes into tetrahedron site, several influences will arise. Firstly, the crystal field splitting will decrease [24,25]. This will enhance the efficient of energy transfer. Secondly, some P site will be blank due to the charge compensation effect, so that the crystal structure of this host will shrink. The distances between each luminescence centre will decrease, which will enhance crystal field. Meanwhile, the emission of Ce^{3+} is easily influenced by crystal field [23]. Within the strong crystal field, spin-orbit splitting of Ce^{3+} ground state

will reduce. This reduction will bring some purple shift to Ce^{3+} emission line, and will enhance the energy transfer from Ce^{3+} to Tb^{3+} [19]. From what has been discussed above, we design a green phosphor based on a Ce^{3+} and Tb^{3+} co-doped $Ca_9La(GeO_4)_{0.75}(PO_4)_6$ (CLGP) system. The phosphor is highly beneficial as it improves the stability of green emission in high temperature and can be used as an emitted material to match AlGaN chip.

Experimental

Materials

$CaCO_3$ (A.R.), $(NH_4)H_2PO_4$(A.R.), GeO_2(A.R.) La_2O_3(4N) CeO_2(4N) and Tb_4O_7 (4N).as raw material are stoichiometric in synthesis process. Aluminum oxide crucibles (10 mm*10 mm) and porcelain boat are utensils for sintering.

Synthesis

Rare earth ions doped samples of CLGP were also prepared by two-step traditional high temperature solid-stated reaction. Preparation of all sample followed same steps. The relative amounts of all materials are calculated by stoichiometric ratio and then weighed by electronic balance accurate to 4 decimal places. None of these material is overweight. Table 1 dedicates the detailed weight ratio of CLGP:$x$$Ce^{3+}$,$y$$Tb^{3+}$, all units are mol.

Table 1 The detailed weight ratio of CLGP:$x$$Ce^{3+}$,$y$$Tb^{3+}$(mol).

	$Ca_9La(GeO_4)_{0.75}(PO_4)_6$:$x$$Ce^{3+}$,$y$$Tb^{3+}$(mol)
$CaCO_3$	9
$(NH_4)H_2PO_4$	6
GeO_2	0.75
La_2O_3	0.5*(1-x-y)
CeO_2	x
Tb_4O_7	0.25y

Put all the raw materials and the flux into agate mortar with 8 mL ethanol added in it at the same time. Grind the mixture for 30 min until they are evenly blended and homogeneous. After the mixture dry, transfer the mixture into aluminum oxide crucibles (10 mm*10 mm) and pre-fire at 500 °C for 2h under air atmosphere. Then, calcine them at 1100 °C for 8h under flowing 95% N_2−5% H_2 atmosphere in the horizontal tube furnace. When they are cooled with 5 °C /min speed to room temperature, grind them to powders, yielding the resulting phosphor powder.

Measurements and characterization

The phase formation and crystal structure were analyzed by the X-ray powder diffraction (XRD) (D2 PHASER X-ray Diffractometer ,Germany) with graphite monochromator using Cu Kα radiation（λ = 1.54056 A), operating at 30 kV and 15 mA. The samples were grinded to powder, then detected by XRD. The investigation range is 10 ° to 80 ° with scanning speed of 15 ° 2θ min^{-1} for the series samples. The photoluminescence (PL) and photoluminescence excitation (PLE) spectra of the samples are measured by a Fluorlog-3 spectrofluorometer (FLS) equipped with 450 W xenon lamps (Horiba Jobin Yvon). The temperature-dependence luminescence properties are measured on the same spectrophotometer, which is combined with a self-made heating attachment and a computer-controlled electric furnace from room temperature (25 °C) to 250 °C with a heating rate of 100 °C/min and a holding time of 5 min for each temperature point. The luminescence decay curves were obtained by FLS-920T fluorescence spectrophotometer as well. A FEI Tecnai G2F30 transmission electron microscope, equipped with a Gatan imaging filter (GIF) system, was used for transmission electron microscopy (TEM). The powder sample is dispersed in alcohol. Then, this solution is dropped onto the carbon film. The carbon film is a base for TEM detecting. All the testes are carried out at room temperature except temperature-dependence luminescence properties testing.

Results and discussion

After preparation and reaction, CLGP, CLGP:0.04Ce^{3+}, CLGP:0.03Tb^{3+} and CLGP:0.04Ce^{3+},xTb^{3+} (x=0-0.04) have been synthesised by solid-state measurement. All the samples are studied by XRD, TEM, FLS to demonstrate its crystal structure and photoluminescence properties.

Crystal Structure of CLGP

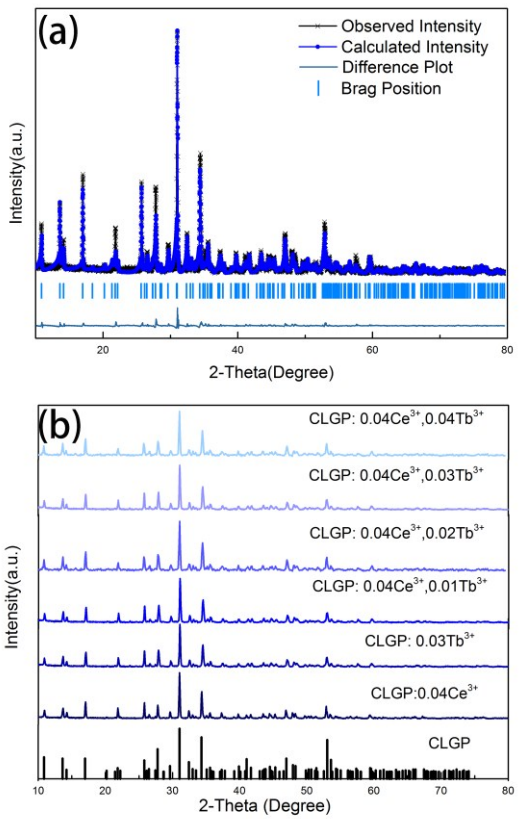

Figure 1 (a) Experimental (crosses), calculated (blue line) and difference (bottom) results of XRD refinement of CLGP host.

(b) The XRD patterns of the samples CLGP, CLGP:xCe,yTb (x=0, 0.04 y=0-0.04).

Figure 1 (a) shows the results of Rietveld refinement for CLGP by TOPAS, which is implemented with the crystallographic information files [25]. The black crosses line is the observed patterns, and the blue solid line is the calculated patterns. The as-obtained goodness of fit parameter Rwp=11.18%, which can confirm the phase's purity.

Figure 1 (b) presents the XRD patterns of the samples CLGP, CLGP:0.04Ce^{3+}, CLGP:0.03Tb^{3+} and CLGP:0.04Ce^{3+}, xTb^{3+} (x=0-0.04). According to the working experience before, all the observed diffraction peaks are well indexed to CLGP without a second phase. We consider that CLGP is prepared by solid-state reaction method, and doping ions do not impact the host structure.

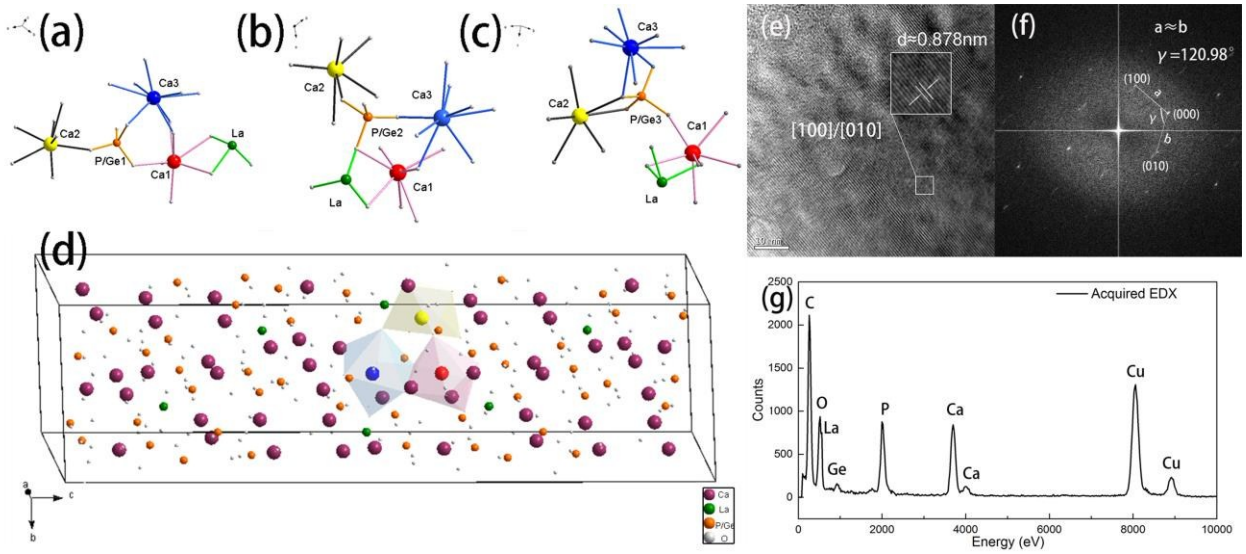

Figure 2(a), (b) and (c) The surrounding information of the different Ca site.(d) The diagram of CLGP according to the refinement. (e)The HRTEM image, (f) the FFT image and (g) the EDX of CLGP.

Figure 2 (a), (b), (c) and (d) show the structure diagram of CLGP according to the refinement. The compound crystalizes is a trigonal crystal system with space group R3c (No. 161). And its cell parameter is a=b=10.40(2) Å, c=37.47(1) Å. All independent Ca^{2+} in CLGP have three different coordination environments. Ca(1) and Ca(2) are both seven-coordinated, while Ca(3) is eight-coordinated. La is three-coordinated and connects to Ca(1) with two O. [25] Every P-O tetrahedron is constituted by one P and four O, and surrounded by three different Ca-O polyhedrons. After Ge-O tetrahedron replaces the site of P-O tetrahedron, a O vacancy will appear randomly. Thus, length between three Ca2+ sites goes down in these area.

Figure 2 (e) and (f) show the HRTEM image, Fast Fourier Transform (FFT) image. Since the theoretical interplanar spacings between (100) and (010) are the same length of 10.40 Å, Figure 2(a) shows the {100} or {010}, and d is the interplanar spacing between (100) and (010). By testing the same area of CLGP, FFT image is shown in Figure 2(b). *a* and *b* in Figure 2(b) are almost same with an angle γ of 120.98°, close to the theoretical value of 120°[25]. By taking FFT image and HRTEM image into consideration, Figure 2(e) shows (001) planes of CLGP.

The EDX analysis is given by Figure 2(g), which confirms the presence of C, O, La, Ge, P, Ca, Cu. C and Cu are from carbon film base. All the information in Figure 2 confirm that the structure and the crystallographic data given by XRD are correct.

Photoluminescence Properties Analysis

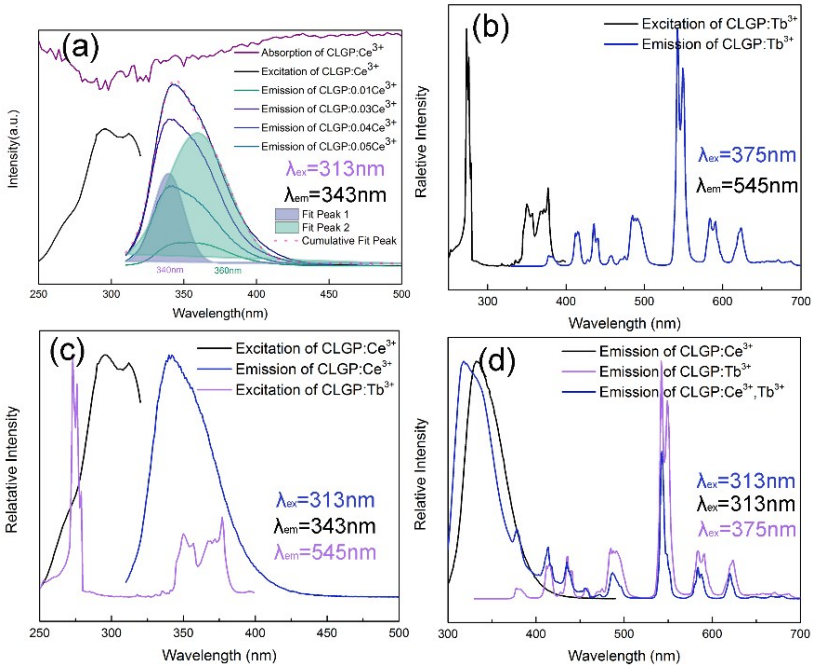

Figure 3 (a) The PLE spectrum and the absorption spectrum of CLGP:Ce, the PL spectra of CLGP:xCe (x=0.01-0.05). (b) The PLE and PL spectra of CLGP:Tb (c) The overlap between PL of CLGP:Ce and PLE of CLGP:Tb (d) The overlap between PL of CLGP:0.04Ce, CLGP:0.04Ce, 0.03Tb and CLGP:0.03Tb^{3+}

Figure 3(a) shows PLE spectrum, absorption spectrum and PL spectra of CLGP:xCe^{3+} (x=0.01-0.05). After using 343nm as monitor, the PLE spectrum of CLGP:Ce^{3+} consists of a board band from 250 to 320nm including two distinct bands peaking at 296nm and 318nm. The absorption spectrum of CLGP:Ce^{3+} also prove the existence of these two peaks, which indicates that phosphor can be effectively excited by the UV light. These two peaks (293nm and 320nm) are attributed to the 4f-5d transition of Ce^{3+}, which has usually spitted into the $^2F_{5/2}$ and the $^2F_{7/2}$ level. The colorized lines in Figure 3(a) shows the PL spectra of CLGP:xCe^{3+} under 313nm excitation depended on concentration, which belongs to transition of 4f-5d of Ce^{3+} [15]. The intensity of emission increases with increasing x until x=0.04.

Figure 3(a) also demonstrates the fitting results of PL spectrum of CLGP:0.04Ce^{3+}. The purple and green area is fitting curves, and the red dot line is the cumulative fit peak by calculating. In order to study the site of Ce^{3+} occupied, we fit the curve with Gaussian deconvolution. After re-calculating the x-scale to cm-1 then transform cm-1 back to nm, the broad band of Ce^{3+} can be decomposed into two Gaussian profiles with two peaks centered at 340nm and 370nm. Using the fitting data(340nm and 370nm)[24], the energy difference between spin-orbit splitting of Ce^{3+} ground state is 2385cm^{-1} based on the calculation, which suits the theoretical value 2000cm^{-1}. This confirms that the asymmetric emission line of Ce is due to the spitted $4f^1$ ground state of Ce^{3+}, and there is only one site for Ce^{3+}, which also confirms the Ce^{3+} only substitutes the occupation of La^{3+}.

The Figure 3(b) shows PL and PLE spectrum of CLGP:Tb^{3+}. The black line in Figure 3(b) is the PLE spectrum of CLGP:Tb^{3+} include four main peaks which are centered at 272nm, 278nm, 350nm and 376nm, respectively. On the basis of reports [26], first two peaks belong to the $^7F_6$-^7D transition and $^7F_6$-^9D transition. The other two peaks at about 350nm and 376nm are supposed to be led by the$^7F_4$-$^5D_2$ transition and $^7F_4$-$^5D_3$ transition [16]. The PL spectrum of CLGP:Tb^{3+} exhibits several peaks from 370nm to 650nm, which confirm the splitting. These peaks are located at 379nm, 414nm(418nm), 435nm(438nm), 487nm(497nm), 545nm(550nm), 584nm(592nm) and 620nm. According to the radius of Ca^{2+} and Tb^{3+}, Tb^{3+} will occupy not only La^{3+} site but Ca^{2+} site as well. Thus, one peaks are splitting into two in distance. As the Tb^{3+} occupied four sites (Ca^{2+} sites and La^{3+} site), this peak is splitting to two peaks. One is the emission of Tb^{3+} sited three Ca^{2+} sites. The first three (379nm, 414nm and 435nm) are brought by $^5D_3$-^7F_J (J=4-6) transition of Tb^{3+}, and the other four (487nm, 545nm, 584nm and 620nm) are led by $^5D_4$-^7F_J (J=3-6) [17]. Among these peaks, the peak sited at 545nm(550nm) owns the highest intensity.

Figure 3(c) presents obvious overlap between PLE spectrum of Tb^{3+}, PL and PLE of Ce^{3+}, which implied that the effective resonance-type energy transfer (ET) could take place from Ce^{3+} to Tb^{3+}. Based on Figure 3(d), the Ce^{3+} emission line of the co-doped CLGP is almost the same as single doped CLGP except a bit red shift. We consider the shift as the re-absorption of Tb^{3+}, which has been reported in other hosts. However, compared with the single doped CLGP, the site of Tb^{3+} emission lines of CLGP:Ce^{3+},Tb^{3+} appear to be no obvious shift.

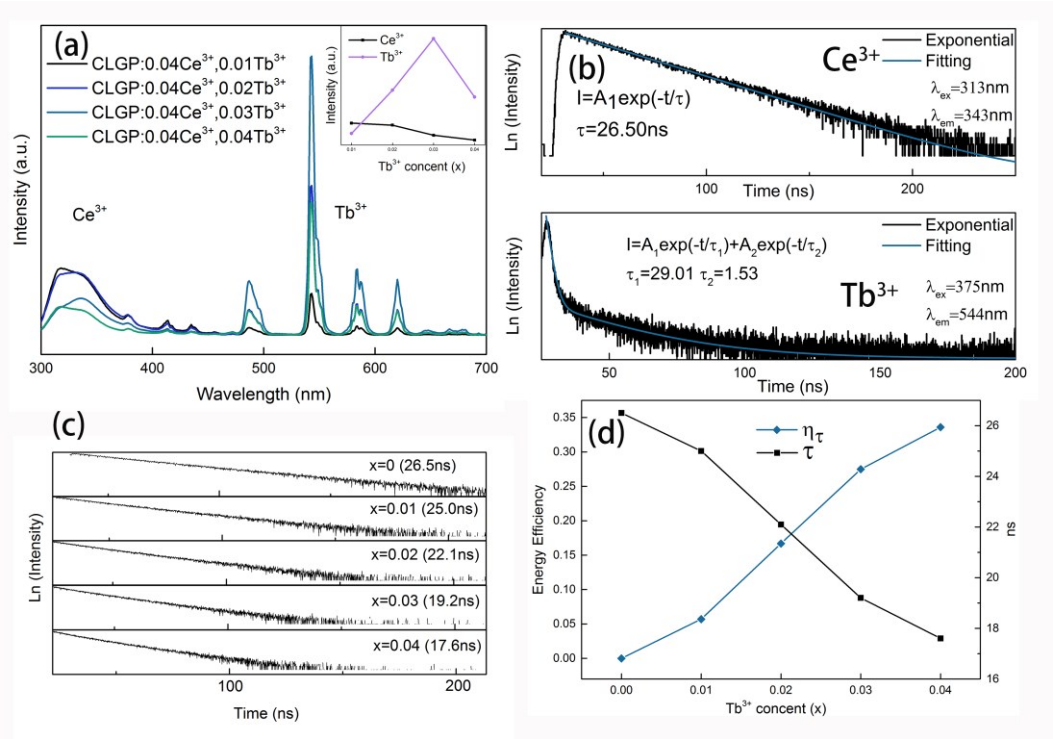

Figure 4 (a) The PL spectra of CLGP:0.04Ce, xTb(x=0.01-0.04) under the excitation of 313nm and the relative intensity of the Ce and Tb emission bands. The inset shows the intensity of C^{+} emission (343nm) and Tb emission (545nm) (b) Decay curve of Ce^{3+} in CLGP:Ce under 313nm excitation monitored at 343nm and decay curve of Tb^{3+} in CLGP:Tb under 375nm excitation monitored at 545nm (c) Decay curve of Ce^{3+} emission in CLGP:0.04Ce, xTb(x=0-0.04) under 313nm excitation and monitored at 343nm. (d) The variation of η_T and τ with the increasing Tb^{3+}

Figure 4(a) shows the PL spectra of CLGP:0.04Ce^{3+},xTb^{3+}(x=0.01-0.04). The line contents a board band centred at 343nm of Ce^{3+} and several peaks of Tb^{3+}. These peaks are from 370nm to 650nm which can be ascribed to $^5D_3$ - ^7F_J (J=0-6) transition and $^5D_4$ - ^7F_J (J=0-6) transition. As can be found, the PL intensity of Ce^{3+} decreases while the emission of Tb^{3+} increases with increasing concentration. These results demonstrate an efficient energy transfer from Ce^{3+} to Tb^{3+}. To further investigate the energy transfer between Ce^{3+} and Tb^{3+}, the decay curves of Ce^{3+} Tb^{3+} are exhibited in Figure 4 (b) and (c). The Figure 4(b) shows the decay time of the single doped CLGP:Ce^{3+} and CLGP:Tb^{3+}. According to Figure 4(b), the decay time of CLGP:Ce^{3+} influenced by only signal exponential, while the decay time of CLGP:Tb^{3+} influenced by double exponential. Thus, it confirms Ce^{3+} only occupies La^{3+} site and Tb^{3+} occupied more than one site. The decay process is characterized by the average lifetime τ, which can be calculated as follow formula [27],

$$\tau = \frac{\left(\int_0^\infty tI(t)dt\right)}{\int_0^\infty I(t)dt}$$

Where I(t) is the luminous intensity at time t. Based on Figure 4(c), the calculated decay times are determined to be 26.5ns, 25.0ns, 22.1ns, 19.2ns and 17.6ns. According to the Dexter's formulation, the ET rate is given by [27]

$$P(R) \propto \frac{Q_A}{R^b \tau_D} \int \frac{f_D(E) F_A(E)}{E^c} dE$$

Where τ_D is the decay time of the donor emission, Q_A is the total absorption cross section of the acceptor ion, R is the distance between the donor and the acceptor, and b and c are parameters dependent on the type of ET. The probability functions $f_d(E)$ and $F_a(E)$ represent the observed shapes of the donor emission band and the acceptor absorption band, respectively. Thus, the ET rate P is in inverse proportion to the decay time τ_D. The energy transfer efficiency $\eta_{Ce\text{-}Tb}$ can be expressed by [28]

$$\eta = 1 - \frac{\tau_s}{\tau_{so}}$$

Where τ_{so} is the lifetime of Ce^{3+} in the absence of Tb^{3+}, and τ_s is the lifetime of the Ce^{3+} in the presence of the Tb^{3+}. As shown in Figure 4(c), the energy transfer efficiency of CLGP:0.04Ce^{3+},xTb^{3+} increase gradually while the x enhances. The η_T are calculated to be 0, 0.057, 0.0167, 0.275 and 0.336, respectively. Figure 4(d) shows the relation between the η_τ and the τ.

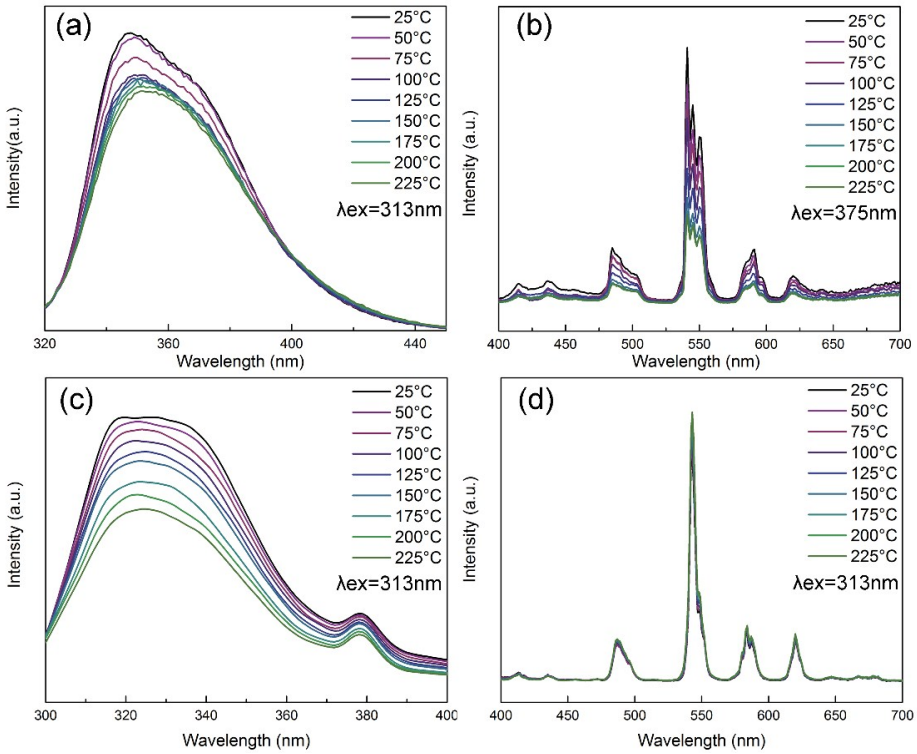

Figure 5 (a) The temperature dependent PL spectra of CLGP:0.04Ce^{3+}, (b) The temperature dependent PL spectra of CLGP:0.03Tb^{3+},(c) The temperature dependent Ce^{3+} emission of CLGP:0.04Ce^{3+},0.03Tb^{3+}, (d) The temperature dependent Tb^{3+} emission of CLGP:0.04Ce^{3+},0.03Tb^{3+}.

Figure 5 shows the temperature dependent PL spectra of CLGP:*x*Ce^{3+},*y*Tb^{3+} (*x*=0/0.04, *y*=0/0.03). A comprehensive understanding of the thermal quenching of phosphor in the process of the phosphors application is indispensable because many devices suffer from thermal problems. The spectra have been measured from 25°C to 225°C. In order to exclude the influence led by thermoluminescence(TL), all spectra are tested from high temperature to room temperature. Additionally, before the test, the samples have been placed into the dark environment of equipment at 225°C for 10min. During the test, all movement and other changes of samples are forbidden, as they may cause the testing environment changed. It can be seen clearly from Figure 5(a) and 5(b), the intensity of single-doped CLGP reduces with the increasing of temperature. However, taking Figure 5(c) and 5(d) into consideration, it is considerable that the co-doped CLGP shows totally different phenomenon in high temperature. Figure 6 is the specific temperature dependent peaks of Figure 5(d).

According to the two black lines in Figure 6 (g), Ce^{3+} emission of CLGP:0.04Ce^{3+} at 225°C reaches 82.5% of its initial intensity at 25°C while Tb^{3+} emission (545nm) of CLGP:0.03Tb^{3+} only attains 34.4%. This phenomenon can be ascribed as thermally active phonon-assisted tunneling from the excited stated of the lower-energy emission to those of the higher-energy emission band in configuration coordinate diagram.

The colourful lines in Figure 6(g) show the normalized PL intensity of CLGP after Ce^{3+} and Tb^{3+}co-doped. The line chart shows different condition while temperature rises. Ce^{3+} emission (343nm) intensity of CLGP:0.04Ce^{3+},0.03Tb^{3+}goes down and drops to 65.7%. However, different peaks of Tb^{3+} emission present different. The intensity of different peaks shows different changing rules. The peaks can be separated into two parts. The lines of first part are below the dash line, which can be attributed to $^5D_3$ - $^7F_6$ (380nm), $^5D_3$ - $^7F_5$ (414nm) and $^5D_3$ - $^7F_4$ (435nm). The other part consist the lines located at 487nm, 545nm, 584nm and 620nm. These peaks are led by transition of $^5D_4$ - ^7F_J (J=6-3). The emission at 545nm reaches 120.4% at 225°C by comparing with its intensity at 25°C.

In general, intensity of peaks in the range between 370nm and 450nm reduces. But the decline of Tb^{3+} emission isn't as much as the Ce^{3+} emission (343nm). By taking Figure 8 and Figure 3(d) into consideration, we regard that the decrease of the first part may be affected by the reduction of Ce^{3+} emission. Since Ce^{3+} line of CLGP:0.04Ce^{3+},0.03Tb^{3+} goes down rapidly and it could extend from 300 nm to 450 nm, Tb^{3+} peaks of the first part reduce in small range. In addition, the Ce^{3+} emission dies out from 370 nm and vanishes at 450 nm. The intensity of Tb^{3+} emission at 343 nm has the most impact and has been lower for the most.

Thus, we consider the peaks of second part are more rigorous without this influence. Which is to say that the thermal quenching doesn't appear in Tb^{3+} emission of CLGP:0.04Ce^{3+},0.03Tb^{3+}. As the phonon-assisted tunneling should still exist in co-doped

CLGP, this unique rising may be caused by ET behaviour. To make this anomaly clear, a reasonable explanation is needed in mechanism.

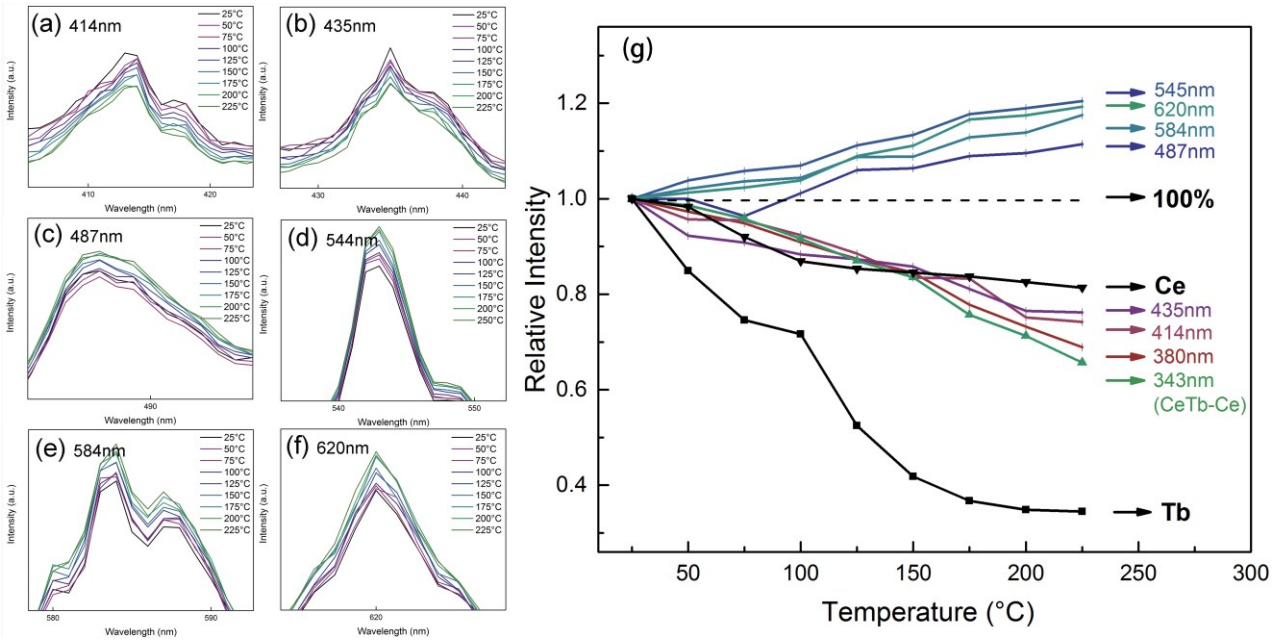

Figure 6 (a)-(f) The specific temperature dependent Tb^{3+} peaks of CLGP: Ce^{3+},Tb^{3+} and (g) The dependence of normalized PL intensities.

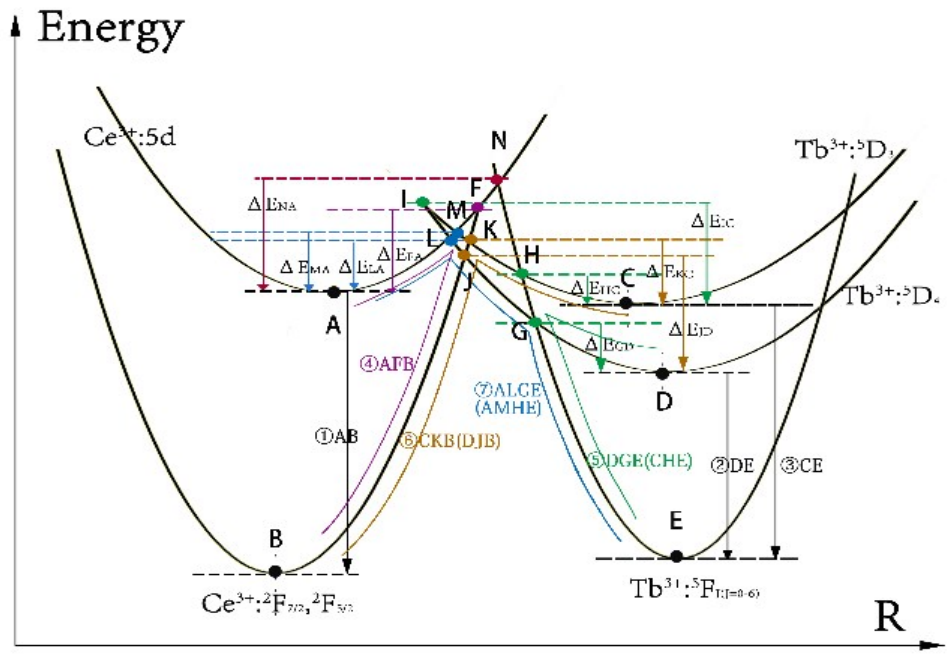

Figure 7 The configurational coordinate diagram of the ground states and the excited states of Ce^{3+} and Tb^{3+}

The traditional stimulated emission channels used for ET couldn't explain this phenomenon, since generally the release of energy is

always shown as the simple drop from excited states to the ground state. The states are described as two parallel lines without any crossing. According to the continuous distribution of electrons, there is no obvious boundary between the ground state and the excited state, and the states should be explained as an area with some overlap. In order to simplify the explanation, we assume the excited states and the ground states of Ce^{3+}, Tb^{3+} are not a content but a function with variable which can be expressed as a curve. In assumption, electron prefers to stay on the position with lower energy, and can only move along the curve in non-radiative transition. [29]

Based on this and the data from spectra, a configurational coordinate diagram has been drawn and shown in Figure 7. The curve AF and BF are the excited and ground state of Ce^{3+} while the CH, DG and EG are the excited and ground state of Tb^{3+}. The energy level splitting of ground states is ignored to simplify the graph. We presume that A and B are the lowest position of the state which they lie in.

Focusing on the situation of single-doped CLGP:Ce^{3+}, the lift part of Ce^{3+} only have one crossing point F (purple point), which is the crossing point of the excited and ground state of Ce^{3+}. According to the emission of Ce^{3+} in Figure 3(a), the site of excited state of Ce^{3+} can be calculated as about $29*10^3$ cm^{-1}. The only electron transition in Ce^{3+}which can release a visible light is to drop follow path①(black line). However, the temperature of environment rises, gives electron the energy to move from A to F. The quantity of electron in F enhances, which will lead more electron to deliver the energy by path4 (purple line). This part of electron will bring no emission in visible area, which can be called as *lost* part. We deem this *lost* part may be the reason why the spectra show thermal quenching.

The transition of CLGP:Tb^{3+} is almost the same as CLGP:Ce^{3+}. C, D and E are the lowest position of $^5D_3$ and $^5D_4$ curve. It is reported that the $^5D_3$ and $^5D_4$ level of Tb^{3+} are about $27*10^3$ cm^{-1} and $21*10^3$ cm^{-1}, respectively. The regular visual emission of Tb^{3+} is brought by $^5D_3$ - ^7F_J and $^5D_4$ - ^7F_J transition. They are draw as path2 and path3 in Figure 7. The *lost* parts of electron in Tb^{3+} is to follow the path5 (green line). During environmental temperature rises, electrons in curve CH free energy by path5 in most cases. Some of them will move to I then land to G. Whereas the ΔE_{IC} is much higher than ΔE_{HC} or ΔE_{GD}, the number of this part is few enough to be overlooked.

The higher temperature generates electron more likely to exist at high energy site. In order to free energy without giving out light, electron in Ce^{3+} should acquire more than ΔE_{FA}, while electron in Tb^{3+} should achieve more than ΔE_{HC} or ΔE_{GD}. From Figure 7, Ce^{3+} emission of CLGP:Ce^{3+} drops less than Tb^{3+} emission (545nm) of CLGP:Tb^{3+} at 225°C, which proof that electrons are more difficult to get to F site than H or G. This means that ΔE_{FA} is higher than ΔE_{HC} or ΔE_{GD}.

When Ce^{3+} and Tb^{3+} are co-doped into CLGP, their state curve will overlap, which gives electrons the opportunities to move from one ion to the other. Since we left out the move from ground state to excited state, the crossing point would be three kinds. The first are the crossing between excited states of Tb^{3+} and excited states of Ce^{3+}, which has been signed as blue point (M and L). The second part are signed as brown point, which are the crossings between excited states of Tb^{3+} and ground states of Ce^{3+}. The third one is the red crossing between excited states of Ce^{3+} and ground states of Tb^{3+}.

For electron in Ce^{3+}, because of the overlap, electron on curve AF now has the new path to release energy by going up to L(M) or N position. ΔE_{NA} is higher than ΔE_{FA}, so the possibility of moving from A to N then drop to E can be ignored. However, ΔE_{LA} and ΔE_{MA} are both lower than ΔE_{FA}, so following path7 (blue line) might be easier than path4. This will bring more electron from AF curve to GD(HC) curve. As the number of electron at excited state increases, the visible emission will enhance despite the lost part. That explains why the intensity of Ce^{3+} emission in CLGP:Ce^{3+},$Tb^{3+}$is much less than it in CLGP:Ce^{3+}. For electron in Tb^{3+}, ΔE_{KC} and ΔE_{JD} are higher than ΔE_{HC} or ΔE_{GD} and more difficult to gain. The electron could have the chance to get enough energy for moving follow the path6 (brown line). Actually, the chance is much lower than the chance to get to H(G) site. So it would be very few electron moves from excited curve of Tb^{3+} to ground curve of Ce^{3+}. That means electrons in Tb^{3+} don't lose too many. The ET between Ce^{3+} and Tb^{3+} still relies mainly on the moving electron from Ce^{3+} to Tb^{3+}, which increases the intensity of Tb^{3+} emission dramatically and reduces the Ce^{3+} emission in CLGP:$0.04Ce^{3+}$,$0.03Tb^{3+}$.

Conclusions

In summary, a simple solid-state route was adopted to fabricate a series of novel phosphor CLGP:Ce^{3+},Tb^{3+}. Their crystal structure, photoluminescence properties, decay times and the thermal properties are discussed in detail. The luminescence analysis demonstrates that the CLGP:Ce^{3+},Tb^{2+} can be efficiently excited by the UV light and simultaneously emit the purple light from Ce^{3+} and the green light from Tb^{3+} and this is attributed to the effective resonance-type Ce^{3+} to Tb^{3+} energy transfer. In the temperature dependent PL spectra, we find an abnormal phenomenon. Compared with the Ce^{3+} and Tb^{3+} single-doped at 220°C, the co-doped leads the emission intensity of Ce^{3+} at 220°C rapidly dropping while the intensity of Tb^{3+} goes up. According to the configurational coordinate diagram, we set up an underlying relationship between thermal quenching and the energy transfer, which can reasonably elucidate the abnormal degradation phenomenon. The results imply the mechanism could be useful for the discussion of the thermal properties of multiple activators co-doped phosphors as reference. Based on this thought, we can ensure the CLGP:$0.04Ce^{3+}$,$0.03Tb^{3+}$ could be a good promising phosphor for its heat stability in green emission area.

Acknowledge

This work is supported by Fundamental Research Funds for the C entral Universities (No. lzujbky-2014-231).

Thanks for the support of Gansu Province Development and Refo rm Commission and Ministry of Industry and Information Techno logy of the Gansu Province.

References

1. R. J. Xie, N. Hirosaki, K. Sakuma, Y. Yamamoto, M. Mitomo, Appl. Phys. Lett., 2004, 84, 5404
2. Nakamura, S., Pearton, S., Fasol, G., Springer. 2000.
3. Madelung, O., Springer Berlin. 1996.
4. Schubert, E. F., Gessmann, T., Kim, J. K., Wiley Online Library. 2005
5. M. Shang, C. Li, J. Lin, Chem. Soc. Reviews, 43(5), 1372-1386..
6. W. Lv, M. Jiao, Q. Zhao, B. Shao, W. Lü, H. You, Inorg. Chem. 2014, 53 (20), 11007.
7. Y. Luo, Z. Xia, J. Phys. Chem. C, 2014, 118 (40), 23297.
8. H. Wu, X. Zhang, C. Guo, J. Xu, M. Wu, Q. Su, Photonics Technology Letters, 2005, 17 (6), 1160.
9. J. L. Reverchon, J. A. Robo , J. P. Truffer, J. P. Caumes, I., Mourad, J. Brault, J. Y. Duboz, International Society for Optics and Photonics, 2007, 9, 674417
10. W. R. Dawson, J. L. Kropp, M. W. Windsor. J. Chem. Phys., 1966, 45(7): 2410-2418
11. Z. L.Wang, Z. W. Quan, P.Y. Jia, C. Lin, Y. Luo, Y. Chen, J. Lin, Chemistry of Materials, 18(8), 2030-2037.
12. M. Yu, J. Lin, J. Fu, H. J. Zhang, Y. C. Han, J. Mater. Chem., 13(6), 1413-1419..
13. M. Chen, Z. Xia, Q. Liu, J. Mater. Chem. C, 3(16), 4197-4204.
14. Z. Xia Z, R.S. Liu. J. Phys. Chem. C, 2012, 116(29): 15604-15609.
15. H. Jiao, Y. Wang J. Electrochemi. Soc., 2009, 156(5): J117-J120.
16. D. Jia, X. J. Wang, W. Jia Appl. Phys., 2003, 93(1): 148-152.
17. C. H. Huang, T. M. Chen, J. Phys. Chem C, 2011, 115(5): 2349-2355.
18. N. El Jouhari, C. Parent, J. C. Zhang. J. De Physique, 1992, 2(2): C2. 257-C2. 260.
19. G. Li, Y. Zhang, D.Geng, Appl. Mater. & Interfaces, 2011, 4(1): 296-305
20. Y. C. Chiu, W.R. Liu, Y. T. Yeh, J. Electrochem. Soc, 2009, 156(8): J221-J225.
21. W. Lü W, Hao Z, Zhang X, et al. Tunable full-color emitting BaMg2Al6Si9O30: Eu2+, Tb3+, Mn2+ phosphors based on energy transfer[J]. Inorganic chemistry, 2011, 50(16): 7846-7851.
22. Blasse G, Bril A. Energy Transfer in Tb3+ - Activated Cerium (III) Compounds[J]. The Journal of Chemical Physics, 1969, 51(8): 3252-3254.
23. 7 C. H. Huang, T. W. Kuo and T. M. Chen, ACS Appl. Mater. Interfaces, 2010, 2, 1395.
24. X. Chen, Z. Xia, Q. Liu, Dalton Trans, 43(35), 13370-13376.
25. P. Berastegui, S. Hull, F. J. G. Garcı J. Solid State Chem. , 2002, 168(1): 294-305.
26. W. Xu, G. Zhu, X. Zhou, Dalton Transact, 2015, 44(19): 9241-9250.
27. D. J. Dexter, J. Chem. Phys., 1953, 21, 836.
28. Y. Tian, B. J. Chen, R. N. Hua, J. S. Sun, L. H. Cheng, H. Y. Zhong, X. P. Li, J. S. Zhang, Y. F. Zheng, T. T. Yu, L. B. Huang, H. Q. Yu, J. Appl. Phys., 2011, 109, 053511.
29. Z. Ci, Q. Sun, M. Sun, X. Jiang, S. Qin, Y. Wang, J. Mater. Chem. C, 2(29), 5850-5856.

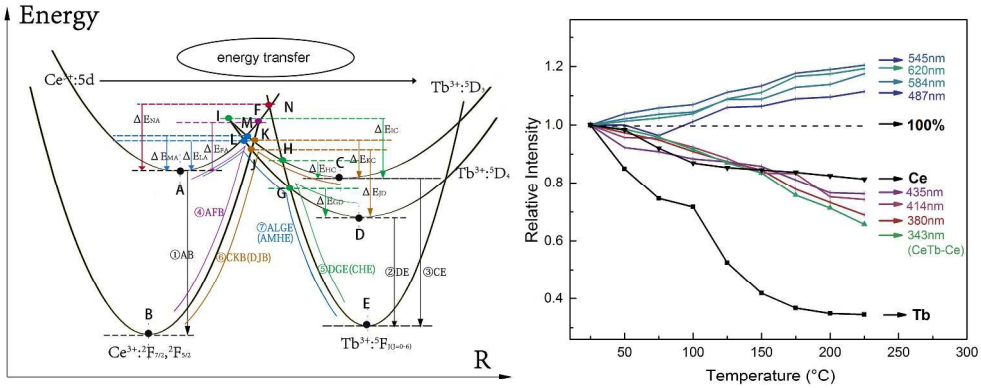

In $Ca_9La(GeO_4)_{0.75}(PO_4)_6$: Ce^{3+}/Tb^{3+}, because of the energy transfer, when temperature increases, intensity of Tb^{3+} shows slightly enhancement instead of thermal quenching.

307x149mm (300 x 300 DPI)